UCB-NE-5004

Effect of Canister-Array Configuration on Release of Long-Lived Fission-Product Species from the Repository

---

D. Kawasaki, J. Ahn, P. L. Chambré

Department of Nuclear Engineering
Univerisity of California
Berkeley, California 94720-1730

May 2004

Contents

List of Figures

1 INTRODUCTION

A high-level radioactive waste repository consists of thousands of waste canisters in a two dimensional array. Groundwater in a water-saturated repository flows along multiple canisters and is contaminated before it flows out from the repository. Analysis on radionuclide transport within the repository plays an important role in the performance assessments for the repository because it determines the inlet boundary condition for the radionuclide transport in the far field.

In previous performance assessments for high-level radioactive waste repository concepts,[3] the radionuclide transport in the groundwater in the engineered-barrier system was first analyzed for a single-canister configuration (independent of other canisters) to determine the radionuclide release rate into the far-field region. The number of waste canisters in the repository was used as a multipication factor to obtain the total radionuclide release from the entire repository. Areal extent of the repository and the canister-array configuration were not reflected in the resulting release rate from the repository.

It was observed in Refs. 1 and 2, however, that the repository size and the canister-array configuration have significant effects on the repository performance for a radionuclide whose release from the waste form is limited by its solubility. Effect of the initial-mass reduction of long-lived radionuclide by partitioning and transmutation technology was investigated in Ref. 1. As mass loading of solubility-limited radionuclide is reduced, the release of the radionuclide evetually becomes congruent to the waste-form degradation. Many fission-product elements are congruently released because of their high solubilities. Developement of high-performance waste forms, that slowly degrade, may also bring congruent release of radionuclides. Thus, the transport analysis of congruently released radionuclides within the repository is important in evaluation of improvement in the waste disposal technology.

The objective of the present study is to investigate transport of a radionuclide congruently released from the waste form, taking into account the canister-array configuration. Transport of a radionuclide in a hypothetical repository is modeled by considering a two-dimensional array of compartments each containing a waste matrix, a buffer, and a Near-Field Rock (NFR) region (Figure 1). Effects of canister-array configuration and leach time on radionuclide release from a repository are investigated numerically and analytically.

2 MODEL

2.1 Repository Structure

In the present model, radionuclide transport in a hypothetical repository in a water-saturated geologic formation is modeled by considering an array of compartments each containing a single waste canister. The waste canisters are placed in a two dimensional array fashion inside the repository. The repository consists of as many compartments as the number of the waste canisters placed in it. The region interior to all compartments is referred to as the *repository* region. The region exterior to the repository is referred to as the *far-field* region.

Schematic diagram of repository structure considered is shown in Figure 1. The repository is partitioned into an $N_x \times N_y$ array of compartments. It is assumed in the present study that the groundwater flows through the repository in the x-direction.[a]

Each compartment consists of a *waste-matrix* region, a *buffer* region, and a *near-field rock* (NFR) region.

The waste matrix is transformed into a slab geometry with the same interfacial area $\hat{S}$ [m^2] [b] as that of the original cylindrical waste canister. The slab waste matrix is assumed to have a width $\hat{d}$ [m], which is the distance between two adjacent waste canisters. To make the surface area of both sides of the slab equal to the original surface area $\hat{S}$, the hypothetical slab height $\hat{H}$ [m] is determined by

$$2\hat{H}\hat{d} = \hat{S}\,.$$

[a] In the case that the water flow is tilted with respect to the compartment array, the two dimensional water flow can be decomposed into x- and y-components. The basic concept of the present model can then be applied to each flow component.

[b] The $\hat{}$ symbol is used to denote quantities with physical dimensions.

It is assumed in this model that the interface between the waste matrix and the buffer, the interface between the buffer and the NFR, the interface between adjacent compartments, and the side boundary are stationary. Each buffer region has the thickness of $\hat{L}$ [m].

Advective groundwater flow is considered in the NFR regions of all compartments. The groundwater flows into the NFR region through one of the interface between two adjacent compartments at rate $\hat{F}$ [m^3/yr], and flows outward through the other at the same rate. The groundwater flowing out from a compartment flows into the NFR region of the next adjacent compartment in the array. The compartments in the repository are thus connected by groundwater flow through the NFR regions. The volumetric flow rate $\hat{F}$ is given by

$$\hat{F} = \hat{\upsilon}\varepsilon_{\mathrm{p}}\hat{A}\,, \tag{1}$$

where $\hat{\upsilon}$ [m/yr] is the pore velocity of the groundwater and ε_{p} is the porosity of the NFR. The cross-sectional area $\hat{A}$ [m^2] between the NFR regions of two adjacent compartments is defined by

$$\hat{A} \equiv \hat{H}\hat{d} = \tfrac{1}{2}\hat{S}\,.$$

The volumetric flow rate $\hat{F}$ is assumed to be constant with time and uniform over the NFR regions of the entire repository. Groundwater in the buffer region is assumed to be stationary, and thus no water flow in the buffer region is considered. The volume $\hat{V}$ [m^3] of the NFR region is defined by

$$\hat{V} \equiv \hat{H}\hat{d}^2\,. \tag{2}$$

The geometry of the repository is considered to be stationary for simplicity, and thus all the dimensions of the regions including $\hat{S}$, $\hat{L}$, and $\hat{V}$ are time-independent.

The buffer and the NFR are considered homogeneously porous. Any void space in the repository and the far-field host rock are assumed to be fully saturated with water. Temperature in the repository would settle down to the ambient temperature[3] by the time the radionuclide release from the waste matrix starts. It is assumed that the ambient temperature in the repository is constant with time.

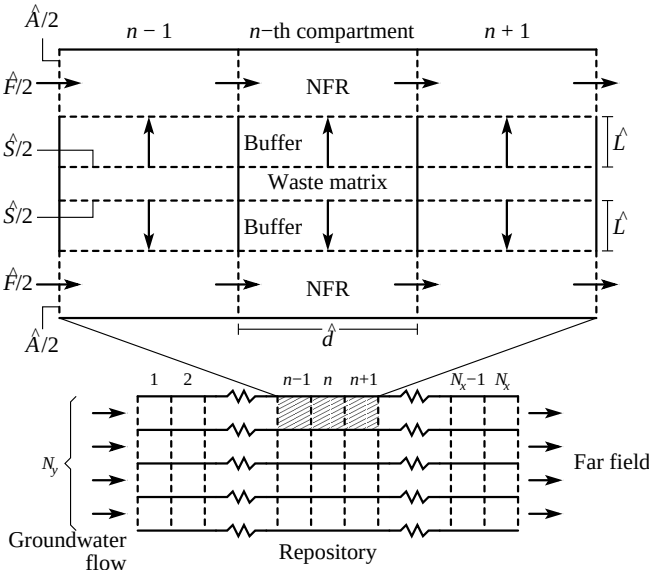

Figure 1 Schematic diagram of repository structure and radionuclide transport considered in the compartment model. Horizontal arrows in the near-field rock (NFR) regions represent advective transport of a radionuclide by groundwater flow. Vertical arrows in the buffer regions represent the radionuclide transport by diffusion. Dashed lines show the boundaries through which the radionuclide can migrate. Solid lines show the boundaries which the radionuclide does not pass across.

2.2 Waste-Matrix Region

In the present study, transport of a single radionuclide, highly soluble in groundwater, is considered. Precursors of a radioactive-decay chain and effects of other isotopes of the element are neglected. [c]

It is assumed that dissolution of the waste matrices in all the compartments begins at time $\hat{t} = 0$ [yr]. Each waste matrix degrades at a constant volumetric rate until it completely dissolves in the groundwater at time $\hat{t} = \hat{T}_{\rm L}$. The matrix degradation is assumed to occur uniformly in all waste forms for simplicity.

There initially exists $\hat{M}^{\circ}$ [mol] of the radionuclide in the waste matrix region of each compartment, and not in the other regions. As the waste matrix degrades, the radionuclide is released congruently from the matrix. The radionuclide released from the matrix is assumed to dissolve immediately in the water phase at waste-matrix/buffer interface. The nuclide is released uniformly over the interfacial area $\hat{S}$.

Mass of the radionuclide in the waste-matrix region, $\hat{M}^{\rm W}(\hat{t})$ [mol], decreases due to radioactive decay and release into the buffer region, and is given as

$$\hat{M}^{\rm W}(\hat{t}) = \begin{cases} \hat{M}^{\circ}\left(1 - \hat{t}/\hat{T}_{\rm L}\right) e^{-\hat{\lambda}\hat{t}}\,, & 0 \le \hat{t} < \hat{T}_{\rm L}\,, \\ 0\,, & \hat{t} \ge \hat{T}_{\rm L}\,, \end{cases} \tag{3}$$

where $\hat{\lambda}$ [yr^{-1}] is the radioactive-decay constant of the radionuclide. The congruent release rate $\hat{q}(\hat{t})$ [mol/yr] from a single waste form is written as

$$\hat{q}(\hat{t}) = \begin{cases} \hat{M}^{\circ} e^{-\hat{\lambda}\hat{t}}/\hat{T}_{\rm L}\,, & 0 < \hat{t} < \hat{T}_{\rm L}\,, \\ 0\,, & \hat{t} \ge \hat{T}_{\rm L}\,. \end{cases} \tag{4}$$

The derivation of Eqs. (3) and (4) are provided in the Appendix A.

2.3 Buffer Region

In the buffer region, transient molecular diffusion of the nuclide is treated in a one-dimensional slab geometry. Advection in the buffer region is neglected because of assumed low permeability in the buffer region. The concentration $\hat{C}_n^{\rm B}(\hat{\xi}, \hat{t})$ [mol/m^3] of the radionuclide in the buffer is governed by the following diffusion equation:

$$K\frac{\partial \hat{C}_n^{\rm B}}{\partial \hat{t}} = \hat{D}\frac{\partial^2 \hat{C}_n^{\rm B}}{\partial \hat{\xi}^2} - \hat{\lambda} K \hat{C}_n^{\rm B}\,,$$
$$0 < \hat{t}\,, \quad 0 < \hat{\xi} < \hat{L}\,, \quad n = 1, 2, \ldots, N_x\,, \tag{5}$$

where $\hat{D}$ [m^2/yr] is the molecular diffusion coefficient of the nuclide, which is assumed to be constant and identical for buffer regions of all compartments. Subscript n denotes the compartment number relative to the upstream side of the repository. It is assumed that all N_y rows of compartments have identical properties, and hence the rows are not specified by notation. Variable $\hat{\xi}$ is the distance from the waste-matrix/buffer boundary. The other boundary $\hat{\xi} = \hat{L}$ is located at the buffer/NFR interface.

Sorption equilibrium between the solid phase and the pore-water phase is assumed. The retardation factor K is defined as

$$K = 1 + \frac{1-\varepsilon}{\varepsilon}\hat{\rho}\hat{K}_{\rm d}\,, \tag{6}$$

where $\hat{\rho}$ [kg/m^3] and ε are the density of the solid matrix material and the porosity in the buffer region, respectively. $\hat{K}_{\rm d}$ [m^3/kg] is the sorption distribution coefficient of the nuclide in the buffer. Parameters $\hat{\rho}$, ε, $\hat{K}_{\rm d}$, and hence K, are assumed to be constant with time and identical in the buffer for all compartments.

It is assumed that there is no radionuclide initially in the buffer. The initial condition for Eq. (5) is written as

$$\hat{C}_n^{\rm B}(\hat{\xi}, 0) = 0\,, \quad 0 < \hat{\xi} < \hat{L}\,, \quad n = 1, 2, \ldots, N_x\,. \tag{7}$$

[c] This applies to most of long-lived FP nuclides. For actinides, a multiple member decay chain may need to be incorporated, depending on the half-lives and sorption retartdation of precursors.

At the waste-matrix/buffer interface ($\hat{\xi} = 0$), the radionuclide is released into the buffer region at rate $\hat{q}(\hat{t})$ given by Eq. (4). The boundary condition for Eq. (5) at the waste-matrix/buffer interface is written as

$$-\hat{S}\varepsilon\hat{D}\frac{\partial\hat{C}_n^{\mathrm{B}}}{\partial\hat{\xi}}\bigg|_{\hat{\xi}=0} = \hat{q}(\hat{t})\,, \quad \hat{t} > 0\,, \quad n = 1, 2, \ldots, N_x\,. \tag{8}$$

Considering the concentration continuity in the water phase at the buffer/NFR interface ($\hat{\xi} = \hat{L}$), the other boundary condition is written as

$$\hat{C}_n^{\mathrm{B}}(\hat{L}, \hat{t}) = \hat{C}_n(\hat{t})\,, \quad \hat{t} > 0\,, \quad n = 1, 2, \ldots, N_x\,, \tag{9}$$

where $\hat{C}_n(\hat{t})$ [mol/m^3] is the uniformized concentration of the nuclide in the pore-water in the NFR region of the n-th compartment, discussed in Section 2.4. The nuclide is released from the buffer into the NFR region according to the diffusive mass flux at the buffer/NFR interface.

The mass $\hat{M}_n^{\mathrm{B}}(\hat{t})$ [mol] of the radionuclide in the buffer region of compartment n is calculated by integrating the concentration and by taking into account both water and solid phases, and is written as

$$\hat{M}_n^{\mathrm{B}}(\hat{t}) = K\varepsilon\hat{S}\int_0^{\hat{L}} \hat{C}_n^{\mathrm{B}}(\hat{\xi}, \hat{t})\,\mathrm{d}\hat{\xi}\,, \quad \hat{t} \geq 0\,, \quad n = 1, 2, \ldots, N_x\,. \tag{10}$$

2.4 Near-Field Rock Region

The nuclide in the NFR region is transported from a compartment to another by advection due to the groundwater flow. The concentration $\hat{C}_n(\hat{t})$ [mol/m^3] of the nuclide in the NFR region of a compartment is uniformized over the pore-water volume in the whole NFR region. It is equivalent to assuming that instantaneous, complete mixing occur in the water phase of the NFR region. The governing equation for the uniformized concentration $\hat{C}_n(\hat{t})$ in the NFR region is formulated as

$$R\varepsilon_{\mathrm{p}}\hat{V}\frac{\mathrm{d}\hat{C}_n}{\mathrm{d}\hat{t}} = -\hat{\lambda}R\varepsilon_{\mathrm{p}}\hat{V}\hat{C}_n + \hat{F}\hat{C}_{n-1} - \hat{F}\hat{C}_n + \hat{Q}(\hat{C}_n, \hat{t})\,,$$
$$\hat{t} > 0\,, \quad n = 1, 2, \ldots, N_x\,, \tag{11}$$

where ε_{p} is the porosity of the NFR region. Volume $\hat{V}$ of the NFR region of a compartment and volumetric flow rate of groundwater, $\hat{F}$, are calculated from Eqs. (2) and (1), respectively. The groundwater flowing into the first compartment is assumed to be uncontaminated, i.e.,

$$\hat{C}_0(\hat{t}) = 0\,, \quad \hat{t} \geq 0\,. \tag{12}$$

The retardation factor R is defined as

$$R = 1 + \frac{1 - \varepsilon_{\mathrm{p}}}{\varepsilon_{\mathrm{p}}}\hat{\rho}_{\mathrm{p}}\hat{K}_{\mathrm{dp}}\,, \tag{13}$$

where $\hat{\rho}_{\mathrm{p}}$ [kg/m^3] is the density of the solid matrix of the porous rock, and $\hat{K}_{\mathrm{dp}}$ [m^3/kg] is the sorption distribution coefficient of the radionuclide for the rock matrix of the NFR. In this formulation, $\hat{V}$, ε_{p}, $\hat{\rho}_{\mathrm{p}}$, $\hat{K}_{\mathrm{dp}}$, and thus R are assumed to be constant with time and identical for all compartments. The first term on the right side of Eq. (11) represents the change of the mass of the radionuclide in the NFR due to radioactive decay. The second and the third terms on the right side represent the mass of the radionuclide flowing in from compartment $n-1$ to compartment n per unit time, and the mass flowing out of compartment n to compartment $n+1$ per unit time by advection. Effect of hydrodynamic dispersion of the nuclide in the flow direction is reproduced by the immediate uniformization of the concentration within an NFR region and the sequence of multiple compartments. The term $\hat{Q}(\hat{C}_n, \hat{t})$ [mol/yr] in Eq. (11) is the release rate of the radionuclide at the buffer/NFR interface into the NFR region, which is written as

$$\hat{Q}(\hat{C}_n, \hat{t}) = -\hat{S}\varepsilon\hat{D}\left.\frac{\partial\hat{C}_n^{\mathrm{B}}}{\partial\hat{\xi}}\right|_{\hat{\xi}=\hat{L}}\,, \quad \hat{t} > 0\,. \tag{14}$$

The right side of Eq. (14) is the diffusive mass release rate at the buffer/NFR interface. The $\hat{C}_n$-dependency of $\hat{Q}(\hat{C}_n, \hat{t})$ arises from that of $\hat{C}_n^{\mathrm{B}}$, which is determined subject to the boundary condition (9). It is assumed that there is no net mass exchange between two adjacent rows of N_x compartments since a radionuclide is released equally in both rows and there will be no concentration gradient between the rows. The governing equation (11) is subject to the following initial condition:

$$\hat{C}_n(0) = 0\,, \quad n = 1, 2, \ldots, N_x\,. \tag{15}$$

The radionuclide released into the NFR region of the first compartment is swept downstream by the uncontaminated water. The radionuclide concentration in the NFR of the second compartment is hence somewhat higher than that of the first compartment since the incoming water is already contaminated. Thus, the concentration in the NFR increases as water flows through the compartments.

The mass $\hat{M}_n^{\mathrm{R}}(\hat{t})$ [mol] of the radionuclide in the NFR region of a single compartment is calculated as

$$\hat{M}_n^{\mathrm{R}}(\hat{t}) = R\varepsilon_{\mathrm{p}}\hat{V}\hat{C}_n(\hat{t})\,, \quad \hat{t} \geq 0\,, \quad n = 1, 2, \ldots, N_x\,. \tag{16}$$

2.5 Release into the Far Field

From the downstream side of the repository region, *i.e.*, from compartment N_x, the radionuclide is released into the far field. The concentration of the radionuclide in the groundwater being released into the far-field region is $\hat{C}_{N_x}(\hat{t})$. Since the groundwater flows at a volumetric rate $\hat{F}$ through each of N_y rows of compartments, the radionuclide release rate $\hat{J}_{N_x,N_y}(\hat{t})$ [mol/yr] from the entire repository is given as

$$\hat{J}_{N_x,N_y}(\hat{t}) = N_y\hat{F}\hat{C}_{N_x}(\hat{t})\,. \tag{17}$$

The mass $\hat{M}^{\mathrm{ext}}(\hat{t})$ [mol] of radionuclide existing in the far field at time $\hat{t}$ is obtained by solving the following mass-balance equation:

$$\frac{\mathrm{d}\hat{M}^{\mathrm{ext}}}{\mathrm{d}\hat{t}} = -\hat{\lambda}\hat{M}^{\mathrm{ext}}(\hat{t}) + \hat{J}_{N_x,N_y}(\hat{t})\,, \quad \hat{t} > 0\,, \tag{18}$$

for which the initial condition is given as

$$\hat{M}^{\mathrm{ext}}(0) = 0\,. \tag{19}$$

Because the repository-exit concentration $\hat{C}_{N_x}(\hat{t})$ is determined by the mass transport in the other upstream compartments by Eq. (11), values of $\hat{J}_{N_x,N_y}(\hat{t})$ and $\hat{M}^{\mathrm{ext}}(\hat{t})$ determined by (17) and (19) include the details of the mass transport in the repository through $\hat{C}_{N_x}(\hat{t})$.

The mass $\hat{M}^{\mathrm{int}}(\hat{t})$ [mol] of the radionuclide in the entire array of N_xN_y compartments in the repository is written as

$$\hat{M}^{\mathrm{int}}(\hat{t}) = N_y\sum_{n=1}^{N_x}\left[\hat{M}^{\mathrm{W}}(\hat{t}) + \hat{M}_n^{\mathrm{B}}(\hat{t}) + \hat{M}_n^{\mathrm{R}}(\hat{t})\right]\,, \quad \hat{t} \geq 0\,. \tag{20}$$

2.6 Conversion into Dimensionless System

We convert the governing equations into dimensionless forms by introducing normalized variables. Time $\hat{t}$ and the position in the buffer, $\hat{\xi}$, are normalized as

$$t \equiv \hat{t}/\hat{T}_1 \quad \text{and} \quad \xi \equiv \hat{\xi}/\hat{L}\,, \tag{21}$$

where $\hat{T}_1$ [yr] is defined as

$$\hat{T}_1 = \frac{R\varepsilon_{\mathrm{p}}\hat{V} + K\varepsilon\hat{S}\hat{L}}{\hat{F}}\,. \tag{22}$$

This time length $\hat{T}_1$ is physically interpreted as the average time that a nuclide, which has entered compartment n from compartment $n-1$, spends in compartment n before it enters downstream compartment $n+1$, for arbitrary n. The average time $\hat{T}_{N_x}$ for the nuclide to migrate across the length of N_x compartments is defined as

$$\hat{T}_{N_x} = N_x\hat{T}_1\,,$$

and the corresponding normalized quantity is

$$T_{N_x} \equiv \hat{T}_{N_x}/\hat{T}_1 = N_x\,.$$

The waste-matrix leach time is normalized with $\hat{T}_1$ as

$$T_{\rm L} \equiv \hat{T}_{\rm L}/\hat{T}_1\,.$$

The masses, concentrations, and release rates are normalized as follow: for $n = 1, 2, \ldots, N_x$,

$$M^{\rm W}(t) \equiv \hat{M}^{\rm W}(\hat{t})e^{\hat{\lambda}\hat{t}}/\hat{M}^\circ\,, \tag{23a}$$
$$M_n^{\rm B}(t) \equiv \hat{M}_n^{\rm B}(\hat{t})e^{\hat{\lambda}\hat{t}}/\hat{M}^\circ\,, \tag{23b}$$
$$M_n^{\rm R}(t) \equiv \hat{M}_n^{\rm R}(\hat{t})e^{\hat{\lambda}\hat{t}}/\hat{M}^\circ\,, \tag{23c}$$
$$M^{\rm int}(t) \equiv \hat{M}^{\rm int}(\hat{t})e^{\hat{\lambda}\hat{t}}/\hat{M}^\circ\,, \tag{23d}$$
$$M^{\rm ext}(t) \equiv \hat{M}^{\rm ext}(\hat{t})e^{\hat{\lambda}\hat{t}}/\hat{M}^\circ\,, \tag{23e}$$
$$C_n^{\rm B}(\xi,t) \equiv \hat{C}_n^{\rm B}(\hat{\xi},\hat{t})e^{\hat{\lambda}\hat{t}}/\hat{C}^\circ\,, \tag{23f}$$
$$C_n(t) \equiv \hat{C}_n(\hat{t})e^{\hat{\lambda}\hat{t}}/\hat{C}^\circ\,, \tag{23g}$$
$$q(t) \equiv \hat{q}(\hat{t})\hat{T}_1 e^{\hat{\lambda}\hat{t}}/\hat{M}^\circ\,, \tag{23h}$$
$$Q(C_n,t) \equiv \hat{Q}(\hat{C}_n,\hat{t})\hat{T}_1 e^{\hat{\lambda}\hat{t}}/\hat{M}^\circ\,, \tag{23i}$$
$$J_{N_x,N_y}(t) \equiv \hat{J}_{N_x,N_y}(\hat{t})\hat{T}_1 e^{\hat{\lambda}\hat{t}}/\hat{M}^\circ\,, \tag{23j}$$

where

$$\hat{C}^\circ \equiv \frac{\hat{M}^\circ}{R\varepsilon_{\rm p}\hat{V} + K\varepsilon\hat{S}\hat{L}}\,. \tag{24}$$

Concentration $\hat{C}^\circ$ can be interpreted as the nuclide concentration for the case that initial mass $\hat{M}^\circ$ is uniformly dispersed over the water phase in the pores of the buffer and the NFR of a single compartment with sorption equilibria between the water phase and the solid phase of the buffer and the NFR.

The dimensionless governing equations are summarized as follow:

$$M^{\rm W}(t) = \begin{cases} 1 - t/T_{\rm L}\,, & 0 \le t < T_{\rm L}\,, \\ 0\,, & t \ge T_{\rm L}\,, \end{cases} \tag{3$'$}$$

$$q(t) = \begin{cases} 1/T_{\rm L}\,, & 0 < t < T_{\rm L}\,, \\ 0\,, & t \ge T_{\rm L}\,. \end{cases} \tag{4$'$}$$

For $n = 1, 2, \ldots, N_x$,

$$(1-\beta)\frac{\partial C_n^{\rm B}}{\partial t} = \gamma\,\frac{\partial^2 C_n^{\rm B}}{\partial \xi^2}\,, \quad 0 < \xi < 1\,, \quad t > 0\,, \tag{5$'$}$$

$$C_n^{\rm B}(\xi,0) = 0\,, \quad 0 < \xi < 1\,, \tag{7$'$}$$

$$-\gamma\,\left.\frac{\partial C_n^{\rm B}}{\partial \xi}\right|_{\xi=0} = q(t)\,, \quad t > 0\,, \tag{8$'$}$$

$$C_n^{\rm B}(1,t) = C_n(t)\,, \quad t > 0\,, \tag{9$'$}$$

$$\beta\frac{{\rm d}C_n}{{\rm d}t} = C_{n-1}(t) - C_n(t) + Q(C_n,t)\,, \quad t > 0\,, \tag{11$'$}$$

$$C_0(t) = 0\,, \quad t > 0\,, \tag{12$'$}$$

$$Q(C_n,t) = -\gamma\,\left.\frac{\partial C_n^{\rm B}}{\partial \xi}\right|_{\xi=1}\,, \quad t > 0\,, \tag{14$'$}$$

$$C_n(0) = 0\,, \tag{15′}$$

$$J_{N_x,N_y}(t) = N_y C_{N_x}(t)\,, \quad t \geq 0\,, \tag{17′}$$

$$\frac{\mathrm{d}M^{\mathrm{ext}}}{\mathrm{d}t} = J_{N_x,N_y}(t)\,, \quad t > 0\,, \tag{18′}$$

$$M^{\mathrm{ext}}(0) = 0\,, \tag{19′}$$

where dimensionless coefficients are defined as [d]

$$\beta \equiv \frac{R\varepsilon_{\mathrm{p}}\hat{V}}{R\varepsilon_{\mathrm{p}}\hat{V} + K\varepsilon\hat{S}\hat{L}}\,, \quad \gamma \equiv \frac{\hat{S}\varepsilon\hat{D}}{\hat{L}\hat{F}}\,. \tag{25}$$

The dimensionless masses in the repository are written as follow: For $t \geq 0$,

$$M_n^{\mathrm{B}}(t) = (1-\beta)\int_0^1 C_n^{\mathrm{B}}(\xi,t)\mathrm{d}\xi\,, \quad n = 1, 2, \ldots, N_x\,, \tag{10′}$$

$$M_n^{\mathrm{R}}(t) = \beta C_n(t)\,, \quad n = 1, 2, \ldots, N_x\,, \tag{16′}$$

$$M^{\mathrm{int}}(t) = N_y \sum_{n=1}^{N_x} \left[M^{\mathrm{W}}(t) + M_n^{\mathrm{B}}(t) + M_n^{\mathrm{R}}(t)\right]\,, \tag{20′}$$

Once the normalized masses and concentrations, M^{W}, M_n^{B}, etc., are obtained from the above equations, they can be converted back to the original quantities with dimensions, $\hat{M}^{\mathrm{W}}$, $\hat{M}_n^{\mathrm{B}}$, etc., by (23a), …, (23j). Note that this set of dimensionless equations do not contain radioactive-decay terms. A solution set for the dimensionless system is valid for multiple isotopes of an element with different half-lives. The form of normalization in (23a) through (23j) also shows that the initial mass $\hat{M}^{\circ}$ only propotionally affects the magnitude of original masses, concentrations, and release rates. Transport in the repository is investigated with the normalized quantities in the following sections.

3 RESULTS AND DISCUSSION

3.1 Input Data

Computer code VR[4] has been used for numerical calculations. The present model is applicable to any long-lived radionuclide that is congruently released from waste forms. The nuclide ^{135}Cs has been chosen for illustration, since it is considered a major contributor to the peak exposure dose rate in the performance assessment of the Japanese repository and it is soluble in groundwater.[3] Parameter values used in the calculation are listed in Table 1. As seen in Eqs. (3′) through (20′), the first five parameters in Table 1 determine the dimensionless system uniquely. Values for these parameters are calculated according to the rest of the parameter values in Table 1.

3.2 Transport in a Single Compartment

We first consider transport of cesium in a repository that consists of a single compartment, i.e., $N_x = N_y = 1$. The dimensionless-concentration profile in the buffer region and the mass distribution in the system have been

[d] The constant β is interpreted as the fraction of the radionuclide mass in the NFR region when a certain mass of the radionuclide is dispersed at a uniform concentration over the buffer and the NFR region. The constant γ can be rewritten as

$$\gamma \equiv \frac{\hat{S}\varepsilon\hat{D}}{\hat{L}\hat{F}} = \frac{\hat{T}_1}{K\hat{L}^2/\hat{D}}(1-\beta)$$

where $\hat{T}_1$ represents the characteristic time for the nuclide to migrate over the length of a compartment in the flow direction, $K\hat{L}^2/\hat{D}$ represents the characteristic time for the diffusion over the buffer thickness, and $1-\beta$ represents the mass fraction in the buffer region when the nuclide is dispersed at a uniform concentration over the buffer and the NFR.

Table 1 Assumed Parameters for Cesium and the Repository

Symbol	Description and Values
N_x	Number of compartments in each row parallel to the groundwater flow
N_y	Number of rows of N_x compartments each in the repository
$T_{\rm L}$	Normalized duration for the waste-matrix dissolution
β	See Eq. (25) (0.96)
γ	See Eq. (25) (0.057)
K	Retardation factor of Cs in the buffer region (50) [a]
R	Retardation factor of Cs in the NFR region (131) [a]
$\hat{T}_{\rm L}$	Duration for the waste-matrix dissolution
$\hat{D}$	Diffusion coefficient for Cs in the buffer ($0.046\,{\rm m}^2/{\rm yr}$) [a,b]
$\hat{F}$	Volumetric flow rate of groundwater through the interface between two adjacent compartments in a row ($0.45\,{\rm m}^3/{\rm yr}$)
ε	Porosity in the buffer region (0.3) [b]
$\varepsilon_{\rm p}$	Porosity in the NFR region (0.5) [b]
$\hat{\rho}$	Density of the solid material in the buffer region ($2100\,{\rm kg/m}^3$) [b]
$\hat{\rho}_{\rm p}$	Density of the solid material in the NFR region ($2600\,{\rm kg/m}^3$) [b]
$\hat{V}$	Volume of the NFR region in a compartment ($9.05\,{\rm m}^3$) [b]
$\hat{\upsilon}$	Pore velocity of groundwater ($1\,{\rm m/yr}$) [b]
$\hat{S}$	Surface area of a single waste matrix ($1.81\,{\rm m}^2$) [b]
$\hat{d}$	Distance between waste canisters (10 m) [b]
$\hat{L}$	Thickness of the buffer region (0.98 m) [b]

[a] See Ref. 3.

[b] See Ref. 5.

obtained by the numerical calculation. The dimensionless-concentration profiles $C_1^{\rm B}(\xi,t)$ of cesium in the buffer region of the compartment are shown in Figure 2 for leach time $T_{\rm L}=73$ ($\hat{T}_{\rm L}=10^5\,{\rm yr}$). The normalized masses $M^{\rm W}(t)$, $M_1^{\rm B}(t)$, $M_1^{\rm R}(t)$, $M^{\rm int}(t)$, and $M^{\rm ext}(t)$ are plotted in Figure 3. The top axis in Figure 3 shows the real physical time $\hat{t}$ corresponding to the normalized time t for the particular parameter values shown in Table 1.

As cesium is congruently released through the waste-matrix/buffer boundary ($\xi=0$ in Figure 2), the mass in the waste matrix, $M^{\rm W}(t)$ in Figure 3, monotonically decreases and becomes zero at $t=T_{\rm L}$. The cesium concentration and its mass $M_1^{\rm B}(t)$ in the buffer region increase. The gradients of the profiles shown in Figure 2 at $\xi=0$ are the same for all the times before $T_{\rm L}$ because of the boundary condition (8′). It is observed in Figure 2 that cesium has reached the outer boundary, $\xi=1$, at $t=0.073$. This implies that the release of the radionuclide from the buffer into the NFR region starts in this time span. The concentration $C_1(t)$ in the NFR, which is equal to $C_1^{\rm B}(1,t)$, is shown in Figure 4.

The concentration $C_1(t)$ and the mass $M_1^{\rm R}(t)$ in the NFR increases thereafter, and gradually levels off until it reaches a steady-state plateau. This steady-state concentration is the peak of $C_1(t)$, and we will refer to the peak level as $C_1^{\rm peak}$. The concentration profile $C_1^{\rm B}(\xi,t)$ in the buffer region also reaches a steady state at the same time, and in Figure 2, the profile for $t=7.3$ is observed to be almost identical to that for $t=73$. The steady state is observed in Figure 3 as the flat plateaus of $M_1^{\rm B}(t)$ and $M_1^{\rm R}(t)$ during $1<t<73$.

During the steady state, the time-derivative term in Eq. (5′) is equal to zero. It follows that the concentration gradient $\partial C_1^{\rm B}/\partial\xi$ is uniform in entire buffer region during the steady state, and hence the release rate of the nuclide from the buffer into the NFR is obtained as $Q=q(t)=1/T_{\rm L}$ from Eqs. (4′), (8′), and (14′). Mass balance in the NFR region [see Eq. (11′) for $n=1$] is maintained between the mass flux from the buffer into the NFR, $Q(C_1,t)$, and the release into the far field, $C_1(t)$. The time-derivative term is equal to zero for the steady state, and $C_0=0$ by Eq. (12′). Therefore the steady-state concentration in the NFR region is obtained from (11′) as

$$C_1^{\rm peak}=1/T_{\rm L}=0.0137\,. \tag{26}$$

At $t=T_{\rm L}$, the congruent release from the waste matrix completes, and the concentrations $C_1^{\rm B}(\xi,t)$, $C_1(t)$, and the masses $M_1^{\rm B}(t)$, $M_1^{\rm R}(t)$ rapidly decrease thereafter.

For the single-compartment repository, the concentration $C_1(t)$ in the NFR region is the nuclide concentration in the water flowing into the far field, and thus it directly affects the radionuclide mass in the far field, $M^{\mathrm{ext}}(t)$. The mass in the far field, $M^{\mathrm{ext}}(t)$, increases until all existing cesium is released from the compartment after $t = T_{\mathrm{L}} = 73$. The mass $M^{\mathrm{int}}(t)$ in the entire repository, which is the sum of $M^{\mathrm{W}}(t)$, $M_1^{\mathrm{B}}(t)$, and $M_1^{\mathrm{R}}(t)$, mostly overlaps with $M^{\mathrm{W}}(t)$. It is observed that curves for $M^{\mathrm{ext}}(t)$ and $M^{\mathrm{int}}(t)$ cross each other at $t = 38$. Before this time the majority of the radionuclide mass exists in the repository, whereas after this time the majority exists in the far field. This time can be considered as the representative residence time of the radionuclide in the repository.

3.3 Transport through Multiple Compartments

3.3.1 Exit Concentration for $N_x < T_{\mathrm{L}}$, $T_{\mathrm{L}} = 73$

The dimensionless concentration $C_{N_x}(t)$ of cesium at the exit of the repository has been obtained by the numerical calculation, and is depicted in Figure 4 for the normalized leach time $T_{\mathrm{L}} = 73$ ($\hat{T}_{\mathrm{L}} = 10^5$ [yr]) and various array configurations. The exit concentration $C_{N_x}(t)$ is common to any value of N_y since there is no interference between two adjacent compartments in the y direction.

For $N_x = 1$, i.e., when there is only one compartment in the x direction, the concentration profiles in the buffer regions and the NFR regions are identical to those observed in the single-compartment repository in Section 3.2 for the above reason. The concentration $C_1(t)$ increases with time in the beginning, and reaches the steady-state level given by Eq. (26). After the congruent release from the waste matrix completes, $C_1(t)$ rapidly decreases to zero.

For $N_x = 2$, a concentration profile similar to that for $N_x = 1$ is observed. The exit concentration $C_2(t)$ increases in the beginning as cesium is released from the waste matrix in the second compartment. The concentration $C_2(t)$, however, reaches a higher value than $C_1(t)$ because cesium accumulates in the flowing water when cesium released from the first compartment flows into the second compartment. Thus, the exit concentration $C_2(t)$ increases for a longer time than $C_1(t)$, and reaches the steady-state level C_2^{peak} twice as high as C_1^{peak}. The steady state lasts until $t = T_{\mathrm{L}}$ and the exit concentration $C_2(t)$ rapidly decreases thereafter as observed in $C_1(t)$.

The same discussion applies to $N_x = 4$, 8, 16, 32, and 64. Because of cesium accumulation in the water over N_x compartments, the exit concentration $C_{N_x}(t)$ increases until the cesium that has been released from the waste form in the first compartment reaches the repository exit. Considering that N_x also represents the normalized time it

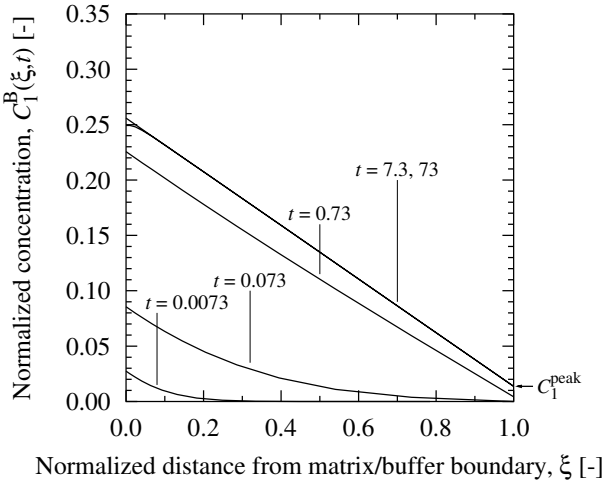

Figure 2 Profile of normalized concentration $C_1^{\mathrm{B}}(\xi, t)$ in the buffer region of the single-compartment repository ($N_x = N_y = 1$). Leach time $T_{\mathrm{L}} = 73$ ($\hat{T}_{\mathrm{L}} = 10^5$ yr).

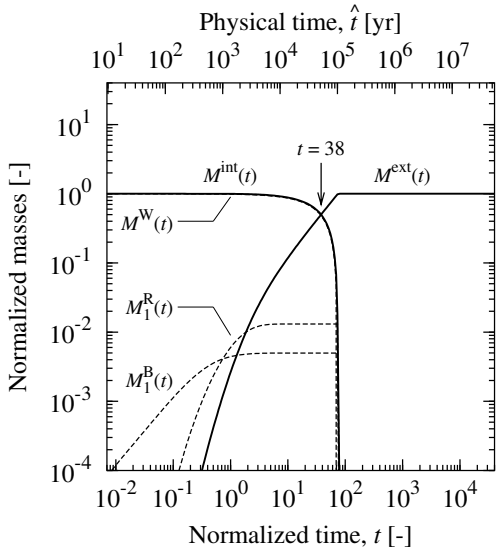

Figure 3 Mass distribution in the single-compartment repository ($N_x = N_y = 1$). Leach time $T_{\mathrm{L}} = 73$ ($\hat{T}_{\mathrm{L}} = 10^5$ yr).

takes for cesium to migrate across the length of N_x compartments, the exit concentration $C_{N_x}(t)$ thus increases until $t \approx N_x$, and its steady state is observed within a time interval $N_x < t < T_L$. For $N_x = 64$, the release of cesium from the waste matrices ceases soon after $C_{64}(t)$ reaches its peak, and thus no time span of a plateau is observed. The spatial distribution of $C_n(t)$ at $t = 73$ obtained by the numerical calculation is shown in Figure 5 for $N_x = 64$, $T_L = 73$. The accumulation of cesium in the water is observed as the linearly increasing concentration along the compartment array in Figure 5. The peak exit concentration $C_{N_x}^{peak}$, corresponding to the steady-state level of $C_{N_x}(t)$, is N_x times as high as C_1^{peak} due to the accumulation of cesium over the compartments.

For the steady state observed during $N_x < t < T_L$, the time-derivative terms in Eqs. (5′) and (11′) are equal to zero. It follows that the concentration gradient $\partial C_n^B/\partial\xi$ is uniform in each buffer region during the steady state, and hence the release rate from the buffer is obtained as $Q = q(t) = 1/T_L$ from Eqs. (4′), (8′), and (14′). Therefore the mass balance equation (11′) is rewritten for the steady state as

$$0 = C_{n-1} - C_n + 1/T_L\,, \quad n = 1, 2, \ldots, N_x\,. \tag{27}$$

Solving (27) for C_n recursively,

$$C_n = C_{n-1} + 1/T_L = C_{n-2} + 2/T_L = \cdots = C_0 + n/T_L = n/T_L\,, \quad n = 1, 2, \ldots, N_x\,, \tag{28}$$

where $C_0 = 0$ [Eq. (12′)] has been applied. With $n = N_x$, the analytical formula for the normalized steady-state concentration, or the peak exit concentration $C_{N_x}^{peak}$, is obtained as

$$C_{N_x}^{peak} = N_x/T_L\,, \quad N_x < T_L\,. \tag{29}$$

3.3.2 Exit Concentration for $N_x > T_L$, $T_L = 7.3$

The normalized exit concentration $C_{N_x}(t)$ obtained by numerical calculation is plotted in Figure 6 for the leach time $T_L = 7.3$ ($\hat{T}_L = 10^4$ [yr]).

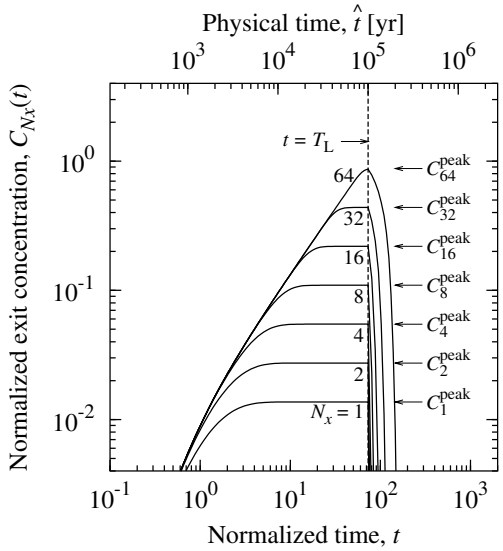

Figure 4 Normalized concentration $C_{N_x}(t)$ of cesium in the groundwater at the repository exit obtained by numerical calculations with VR code. Normalized leach time $T_L = 73$ ($\hat{T}_L = 10^5$ [yr]). Canister-array configuration $N_x = 1$, 2, 4, 8, 16, 32, and 64. Note that the exit concentration $C_{N_x}(t)$ does not depend on N_y. See Table 1 for other parameter values.

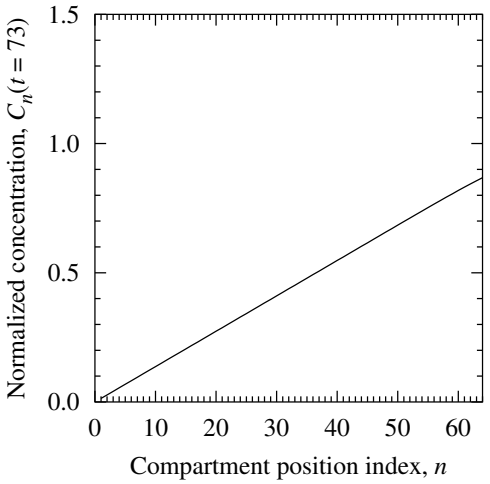

Figure 5 Spatial distribution of $C_n(t)$ along the groundwater flow stream at time $t = 73$ ($\hat{t} = 10^5$ yr) for $N_x = 64$ and $T_L = 73$.

For $N_x = 1$, 2, and 4, the cesium released from the first compartment reaches the repository exit before the congruent release from the waste matrices ceases, i.e., $N_x < T_L$. The exit concentration $C_{N_x}(t)$ approaches a steady-state level, and rapidly decreases after $t = T_L$ as observed for the case of $T_L = 73$ in Figure 4. The peak concentration $C_{N_x}^{peak}$ proportionally increases with N_x for these configurations, and is formulated as Eq. (29).

For $N_x = 16$, 32, and 64, the exit concentration increases until the congruent release from the waste matrix completes at $t = T_L$, and is maintained at a plateau level for some time after T_L. The plateau levels for $N_x = 16$, 32, and 64 are observed identical to each other. The exit concentration begins to decrease at $t \approx N_x$.

The configuration of $N_x = 8$ shows an intermediate concentration profile between the aforementioned two groups.

Figures 7 and 8 show the spatial distribution of the concentration $C_n(t)$ in the NFR regions along the compartment row, and the spatial distribution of $C_{64}^B(\xi, t)$ in the buffer region of the last (64th) compartment, respectively, for $N_x = 64$ and $T_L = 7.3$. During $0 < t < T_L$, the normalized concentration $C_n(t)$ increases at the same rate in the compartments near the repository exit (downstream compartments) as cesium is released from the waste matrices at the same rate in each compartment ($t = 0.2T_L$ and $0.5T_L$). During this early time domain, there is no concentration difference between two adjacent compartments near the repository exit. In such a case, the difference $C_{n-1}(t) - C_n(t)$ in Eq. (11′) is equal to zero, and Eq. (11′) becomes

$$\beta \frac{dC_n}{dt} = Q(C_n, t)\,. \tag{30}$$

Thus, increase in $C_n(t)$ with time is only due to the mass flux Q from the buffer region.

The mass balance equation over the entire buffer region is obtained by integrating Eq. (5′) over $\xi \in [0, 1]$:

$$(1-\beta)\int_0^1 \frac{\partial C_n^B}{\partial t} d\xi = q(t) - Q(C_n, t)\,, \quad t > 0\,, \tag{31}$$

where Eqs. (8′) and (14′) have been applied. Note that the left-side terms in Eqs. (30) and (31) represent the rates of mass change, dM_n^R/dt in the NFR and dM_n^B/dt in the buffer, respectively, since $M_n^R(t)$ and $M_n^B(t)$ are given by Eqs. (16′) and (10′). Integrating the sum of Eqs. (30) and (31) over time, the total mass of the nuclide in the buffer

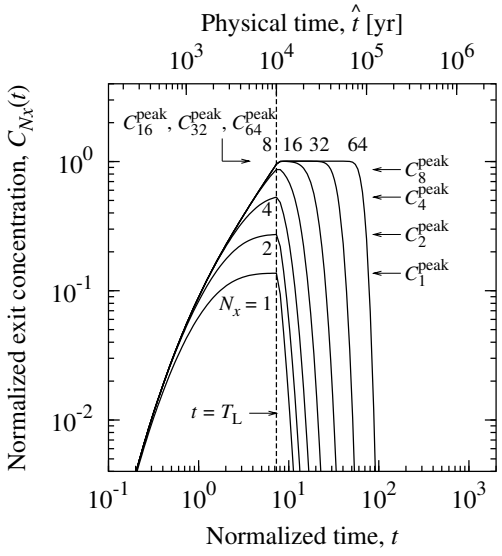

Figure 6 Normalized concentration $C_{N_x}(t)$ of cesium in the groundwater at the repository exit obtained by numerical calculations with VR code. Normalized leach time $T_L = 7.3$ ($\hat{T}_L = 10^4$ [yr]). Canister-array configuration $N_x = 1$, 2, 4, 8, 16, 32, and 64.

region and the NFR region after $t = T_{\rm L}$ is obtained as

$$\begin{aligned}\beta C_n(t) + (1-\beta)\int_0^1 C_n^{\rm B}(\xi,t)\mathrm{d}\xi &= \int_0^t q(t')\mathrm{d}t' \\ &= \int_0^{T_{\rm L}} (1/T_{\rm L})\,\mathrm{d}t' \\ &= 1\,, \quad T_{\rm L} \le t < N_x\,, \end{aligned} \tag{32}$$

where Eq. (4′) has been applied to obtain the expression of $q(t')$ in the right side. Replacing the terms in the left side with $M_n^{\rm B}(t)$ and $M_n^{\rm R}(t)$ given in Eqs. (10′) and (16′), the above equation can be rewritten as

$$M_n^{\rm R}(t) + M_n^{\rm B}(t) = 1\,, \quad T_{\rm L} \le t < N_x\,. \tag{33}$$

The unity on the right side corresponds to the initial amount of the nuclide in a canister. Thus, the same amount of the nuclide as is initially loaded in a single canister exists in the combined region of the buffer and the NFR in a compartment after the nuclide is completely released from the waste matrix. This mass balance is maintained as long as there is no concentration difference between the two adjacent compartments.

In Figure 8, a spatially uniform concentration has been observed in the buffer region and the NFR region of the last compartment of the repository after $t = T_{\rm L}$. This uniform concentration corresponds to the peak exit concentration $C_{64}^{\rm peak}$ shown in Figure 6, which forms the plateau observed during $T_{\rm L} < t < N_x$:

$$C_{N_x}^{\rm B}(\xi,t) = C_{N_x} = C_{N_x}^{\rm peak}\,, \quad 0 \le \xi \le 1\,, \quad T_{\rm L} < t < N_x\,. \tag{34}$$

The mass flux Q at the buffer/NFR interface is equal to zero since the concentration gradient at the interface is zero. Therefore, the right side of Eq. (11′) is zero because, as we discussed prior to Eq. (30), the concentration difference $C_{N_x-1}(t) - C_{N_x}(t)$ is also equal to zero, and $C_{N_x}(t)$ is thus maintained at the constant level $C_{N_x}^{\rm peak}$ ($t = 2T_{\rm L}$, $4T_{\rm L}$, and $6T_{\rm L}$ in Figure 7). Applying Eq. (34) to Eq. (32), the normalized peak concentration $C_{N_x}^{\rm peak}$ for $N_x > T_{\rm L}$ is obtained as

$$C_{N_x}^{\rm peak} = 1\,, \quad N_x > T_{\rm L}\,. \tag{35}$$

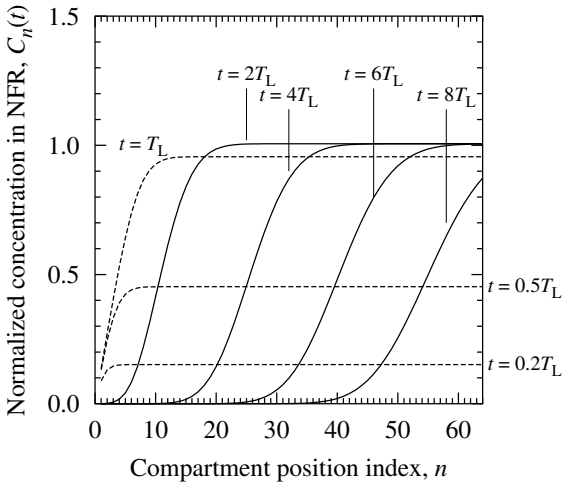

Figure 7 Spatial distribution of the normalized concentration $C_n(t)$ of cesium along the groundwater-flow stream for $N_x = 64$ and $T_{\rm L} = 7.3$ ($\hat{T}_{\rm L} = 10^4$ [yr]). The dashed lines and the solid lines represent concentration profiles for $t \le T_{\rm L}$ and for $t > T_{\rm L}$, respectively.

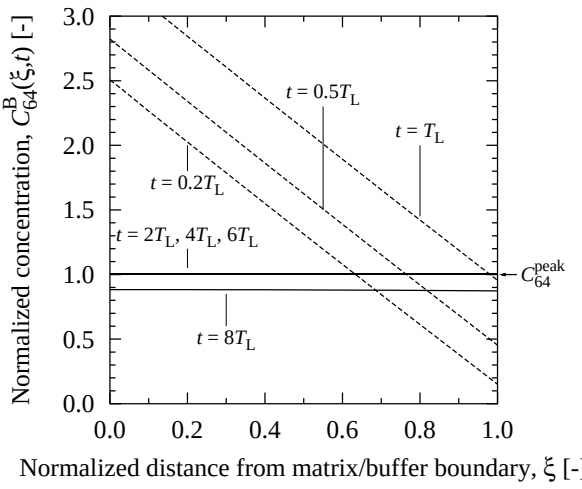

Figure 8 Spatial distribution of the normalized concentration $C_{64}^{\rm B}(\xi,t)$ of cesium in the buffer region of the 64th compartment. $N_x = 64$ and $T_{\rm L} = 7.3$. The dashed lines and the solid lines represent concentration profiles for $t \le T_{\rm L}$ and for $t > T_{\rm L}$, respectively.

This dimensionless concentration $C_{N_x}^{\mathrm{peak}} = 1$ corresponds to $\hat{C}^{\circ}$ [mol/m^3] defined in Eq. (24). It can be interpreted as the concentration in case the initial mass of the radionuclide loaded in a single canister all dissolved in the buffer region and in the NFR region of a compartment uniformly. The magnitude of the peak concentration given by Eq. (35) does not depend on the number of canisters, N_x, or on the leach time T_{L}. Note that $\hat{C}^{\circ}$ is determined by the initial mass loading of the radionuclide in a single canister, the volumes of the pore water in the buffer region and the NFR region of a compartment, and the sorption properties of the radionuclide in the media.

In the upstream side of the compartment array, cesium is swept away towards downstream compartments by the fresh water entering the repository (Figure 7). The concentration $C_n(t)$ decreases to zero after the cesium from the first compartment passes through the compartment. The concentration $C_{64}(t)$ in the last compartment of the repository is kept constant until the cesium that has been released from the first compartment reaches the last compartment at $t \approx 64$. The flow rate of cesium from the upstream compartment $n = 63$ rapidly decreases thereafter, and the exit concentration $C_{64}(t)$ decreases accordingly. Thus, the peak exit concentration given by Eq. (35) is maintained until $t \approx N_x$.

3.3.3 Peak Exit Concentration and Its Upper Bound

Two types of the peak exit concentration $C_{N_x}^{\mathrm{peak}}$ [Eqs. (29) and (35)] have been observed depending on values of N_x and T_{L}. The peak value $C_{N_x}^{\mathrm{peak}}$ for $T_{\mathrm{L}} = 7.3$ based on the analytical formulae is plotted in Figure 9 as a function of N_x.

The peak values obtained from numerical calculation by the VR code are also shown in the figure by the dashed line. The analytical results agree to the numerical results except for deviation observed in the vicinity of $N_x = T_{\mathrm{L}}$, in which case the length of the plateau period of $C_{N_x}(t)$ is very short and the peak level of the concentration is reduced by the dispersion effect in the flow direction.

The peak exit concentration $C_{N_x}^{\mathrm{peak}}$ increases proportionally with N_x for $N_x < T_{\mathrm{L}}$ [Eq. (29)], and becomes constant regardless of the value of N_x if the number N_x of connected canisters is greater than T_{L} as shown in Eq. (35). This means that $C_{N_x}^{\mathrm{peak}}$ given by Eq. (35) can be considered as a theoretical *upper bound* of the exit concentration for any number of connected compartments. As shown in Figure 9, the peak exit concentration $C_{N_x}^{\mathrm{peak}}$ for any value of N_x

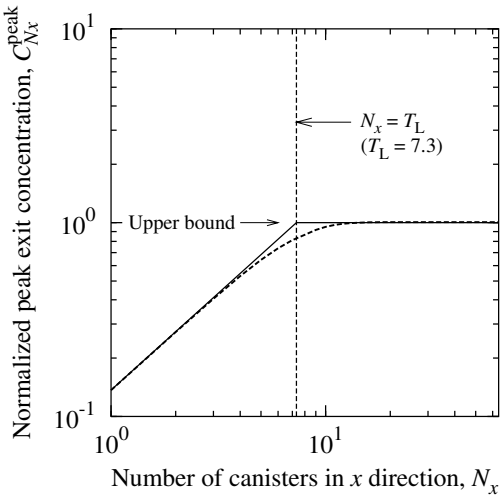

Figure 9 The peak exit concentration $C_{N_x}^{\mathrm{peak}}$ of cesium obtained from analytical formulae (29) and (35) for $T_{\mathrm{L}} = 7.3$ (solid line) and that from numerical transient calculation (dashed line).

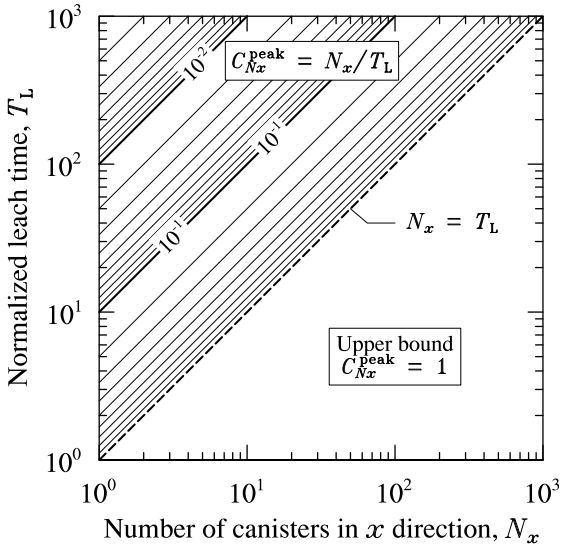

Figure 10 Contour plot of the peak exit concentration as a function of the normalized leach time T_{L} and N_x. The contour levels are shown in the logarithmic scale. The value of $C_{N_x}^{\mathrm{peak}}$ is equal to the constant upper bound given by Eq. (35) in the lower-right region ($N_x > T_{\mathrm{L}}$).

never exceeds the value given by Eq. (35). (This can also be confirmed with the numerical results shown in Figure 6 as the fact that $C_{N_x}(t)$ never exceeds the upperbound value.) Note that it was considered in previous performance assessments[3] that the concentration of a congruently-released radionuclide increases proportionally with the number of canisters without such an upper bound.

The N_x- and $T_{\rm L}$-dependence of the peak exit concentration is depicted in Figure 10 as a contour plot of $C_{N_x}^{\rm peak}$. There are two regions, the upper-left region ($N_x < T_{\rm L}$) and the lower-right region ($N_x > T_{\rm L}$), separated by a straight line $N_x = T_{\rm L}$ in the figure. In the upper-left region, $C_{N_x}^{\rm peak}$ is determined by Eq. (29), and decreases as $T_{\rm L}$ becomes greater and as N_x becomes less. Different designs of canister-array configuration in the repository can lead to different magnitudes of $C_{N_x}^{\rm peak}$ in this region. The peak concentration $C_{N_x}^{\rm peak}$ is also sensitive to $T_{\rm L}$, and the uncertainty of $T_{\rm L}$ value is reflected in the uncertainty of $C_{N_x}^{\rm peak}$.

In the lower-right region, $C_{N_x}^{\rm peak}$ is determined by Eq. (35), and is constant at unity everywhere in the region. The peak concentration $C_{N_x}^{\rm peak}$ in this region does not depend on the matrix leach-time $T_{\rm L}$ or the number N_x of the connected compartments. This implies that the peak exit concentration for $N_x > T_{\rm L}$ is free from uncertainty originating in the variations in $T_{\rm L}$. This result also implies that there is no difference in the concentration of the radionuclide in out-going water once the repository size (N_x) exceeds the threshold ($T_{\rm L}$). Differences in $T_{\rm L}$ and N_x due to different designs of the waste forms and repository configuration do not lead to a difference in $C_{N_x}^{\rm peak}$ as long as N_x is greater than $T_{\rm L}$.

3.4 Effects of Canister-Array Configuration

Effects of canister-array configuration are discussed in this section. For this purpose, three different configurations depicted in Figure 11 are mainly considered. The repository contains 64 compartments for each configuration. Values of the (N_x, N_y)-pair are assigned for configuration A, B, and C as $(64, 1)$, $(8, 8)$, and $(1, 64)$, respectively. The matrix leach time is set to $T_{\rm L} = 7.3$ throughout this section.

3.4.1 Exit Concentration and Release Rate from the Repository

The exit concentration $C_{N_x}(t)$ and the release rate $J_{N_x,N_y}(t)$ obtained from numerical calculations by the VR code are shown in Figures 12 and 13, respectively. The release rate $J_{N_x,N_y}(t)$ has been obtained from the values of $C_{N_x}(t)$ using Eq. (17′).

The exit concentrations for configurations A, B, and C correspond to those shown in Figure 6 for $N_x = 64$, 8, and 1, respectively. Note that $C_{N_x}(t)$ does not depend on the value of N_y. The exit concentration in configuration A reaches the upperbound level formulated in Eq. (35), and the release from the repository lasts longer than those for other configurations. The exit concentration in configuration C is the lowest among three configurations at any time,

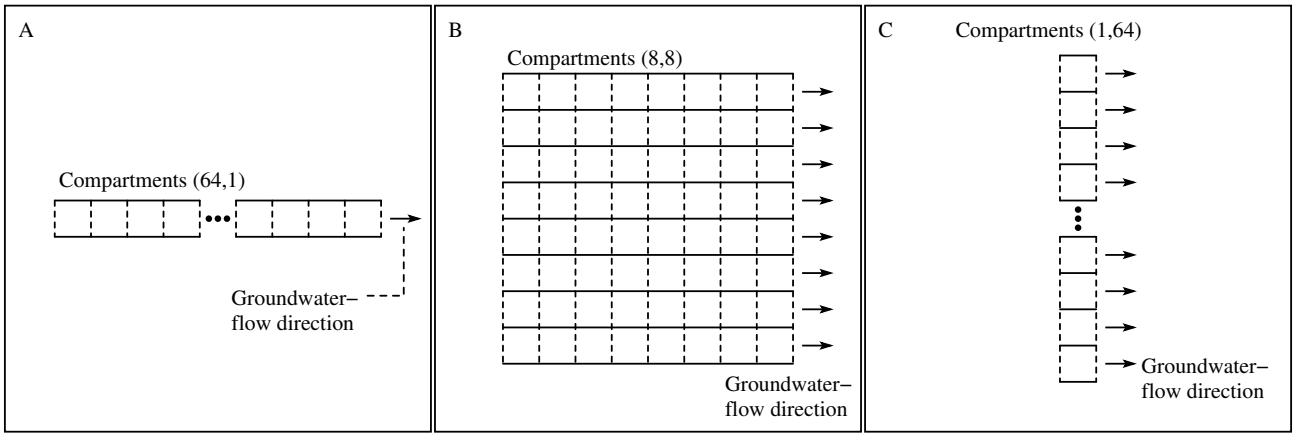

Figure 11 Compartment-array configurations in the repository. The values of (N_x, N_y) are $(64, 1)$, $(8, 8)$, and $(1, 64)$ for configuration A, B, and C, respectively. All configurations contain 64 waste canisters ($N_x N_y = 64$).

and its peak level is formulated in Eq. (29). The characteristics observed in the profile of the exit concentration are thus different for different configurations, even though the total number of waste canisters in the repository is the same. The essential difference between configurations A and C is the orientation of the canister-array arrangement relative to the direction of the groundwater flow. Thus, the orientation of the array is an important factor that determines the exit concentration.

In contrast to the low exit concentration for configuration C, the release rate $J_{N_x,N_y}(t)$ for configuration C reaches the highest peak level. This is because the cross-sectional area of the groundwater stream that flows through the repository of configuration C is 64 times greater than that of configuration A, but the peak exit concentration for configuration C is less than that for configuration A only by factor of 0.137 ($> 1/64$). It is observed that cesium is released from the repository in a short period of time in configuration C. In configuration A, cesium is released slowly over a long period of time despite the high exit concentration.

3.4.2 Peak Release Rate

The normalized peak release rate from the entire repository, $J^{\text{peak}}_{N_x,N_y}$, can be derived from Eq. (17′) as

$$J^{\text{peak}}_{N_x,N_y} = N_y C^{\text{peak}}_{N_x}. \tag{36}$$

Values of $J^{\text{peak}}_{N_x,N_y}$ are obtained by substituting the analytical formulae (29) and (35) into the above equation, and are plotted in Figure 14 with the total number of canisters in the repository fixed to 64. The value of N_y uniquely corresponds to that of N_x through this condition of fixed total number, $N_x N_y = 64$.

In contrast to the peak exit concentration $C^{\text{peak}}_{N_x}$ shown in Figure 9, the peak release rate $J^{\text{peak}}_{N_x,N_y}$ is independent of the canister-array configuration for $N_x < T_{\text{L}}$, and decreases with N_x for $N_x > T_{\text{L}}$. It follows that $J^{\text{peak}}_{N_x,N_y}$ takes the highest value in the configuration C [$(N_x, N_y) = (1, 64)$] even though $C^{\text{peak}}_{N_x}$ in Figure 9 becomes the lowest concentration. On the other hand, $J^{\text{peak}}_{N_x,N_y}$ becomes the lowest release rate in the configuration A while $C^{\text{peak}}_{N_x}$ is equal to its upper-bound level. Thus, the repository performance evaluation based on the exit concentration and that based on the mass release rate from the repository appear to have different dependence on canister-array configuration.

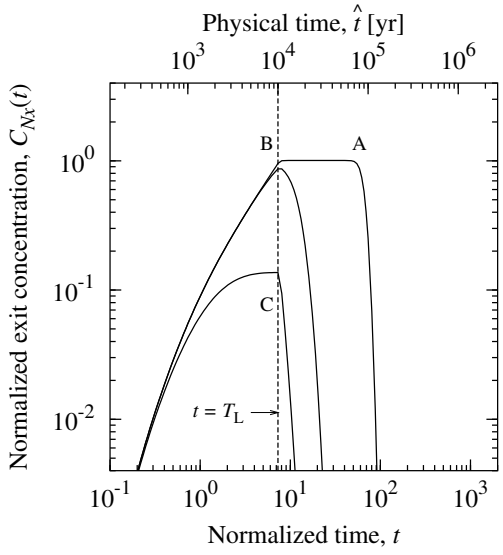

Figure 12 Normalized exit concentration $C_{N_x}(t)$ for configurations A, B, and C. The matrix leach-time $T_{\text{L}} = 7.3$.

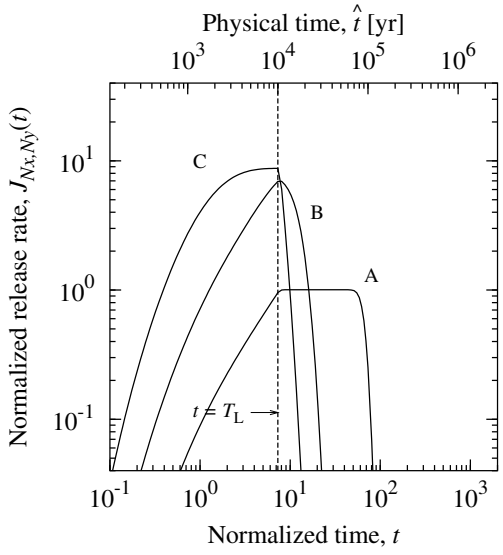

Figure 13 Normalized release rate $J_{N_x,N_y}(t)$ from the repository for configurations A, B, and C. The matrix leach-time $T_{\text{L}} = 7.3$.

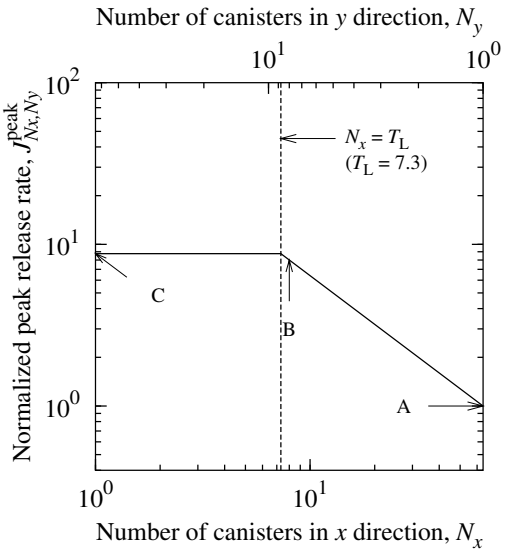

Figure 14 The peak release rate $J^{\rm peak}_{N_x,N_y}$ of cesium from the entire repository obtained from analytical formula (36) for $T_{\rm L} = 7.3$. The total number of canisters in the repository is fixed to 64 ($N_x N_y = 64$).

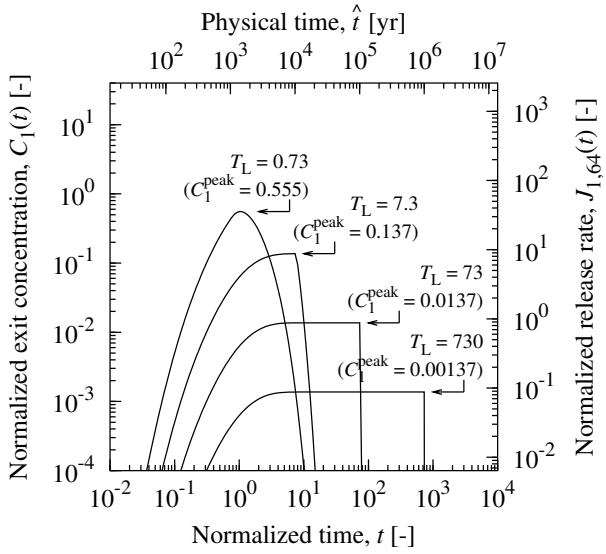

Figure 15 Normalized concentration $C_1(t)$ of cesium in the groundwater exiting the repository of configuration C and the corresponding normalized release rate $J_{1,64}(t)$ into the far field. Concentrations for leach time $T_{\rm L} = 0.73$, 7.3, 73, and 730 are plotted in solid lines.

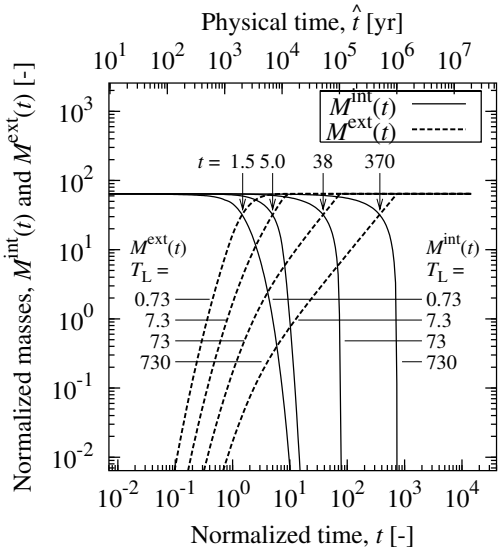

Figure 16 Normalized masses of cesium, $M^{\rm int}(t)$ in the repository and $M^{\rm ext}(t)$ in the far field for configuration C. Mass $M^{\rm int}(t)$ for leach time $T_{\rm L} = 0.73$, 7.3, 73, and 730 is plotted in solid lines. Mass $M^{\rm ext}(t)$ in the far field is plotted in dashed lines.

3.5 Effects of Leach Time

Figure 15 shows the exit concentrations $C_1(t)$ and the release rates $J_{1,64}(t)$ from the repository of configuration C for varous values of $T_{\rm L}$. Figure 16 shows the corresponding mass-distribution profiles in the repository and in the far field region.

According to the discussions in Section 3.3, the peak levels of the exit concentration for $T_{\rm L} = 7.3$, 73, and 730 (greater than $N_x = 1$) are analytically obtained as $C_1^{\rm peak} = 1/T_{\rm L}$. The inverse proportionality between $T_{\rm L}$ and $C_1^{\rm peak}$ for these cases is also confirmed in Figure 15, as the plateau level decreases as $T_{\rm L}$ becomes greater. It is also observed that the release of the radionuclide into the far field lasts longer for a greater value of $T_{\rm L}$. These effects are reflected in the mass distributions in Figure 16 as the residence time of the nuclide in the repository. The representative residence time, which is the time when $M^{\rm int}(t)$ and $M^{\rm ext}(t)$ cross each other, is observed to increase according to $T_{\rm L}$.

The exit concentration $C_{64}(t)$ and the mass distribution for configuration A are shown in Figures 17 and 18, respectively.

For $T_{\rm L} = 73$ and 730 (greater than $N_x = 64$) in configuration A, the similar effect of the inverse proportionality between $T_{\rm L}$ and $C_{64}^{\rm peak}$ and the difference in the residence times are observed. For $T_{\rm L} = 0.73$ and 7.3 (less than $N_x = 64$), however, the peak levels of $C_{64}(t)$ are constant at the upperbound value given by Eq. (35). No significant difference is observed in the end time of the release from the repository between $T_{\rm L} = 0.73$ and 7.3. Only a slight difference is observed in the representative residence time between $T_{\rm L} = 0.73$ and 7.3, whereas that between $T_{\rm L} = 73$ and 730 is significant. It is observed that the concentration for $T_{\rm L} = 0.73$ rises and reaches the plateau earlier than that for $T_{\rm L} = 7.3$. This means that the release of the radionuclide into the far field starts earlier for shorter leach time.

Thus, if the matrix leach-time $T_{\rm L}$ is less than the threshold value N_x, change in $T_{\rm L}$ would make no effect on the peak values $C_{N_x}^{\rm peak}$ and $J_{N_x,N_y}^{\rm peak}$, and only a slight difference in the residence time of the nuclide in the repository is observed. If $T_{\rm L}$ is greater than the threshold value N_x, increase in $T_{\rm L}$ would inverse-proportionally reduce $C_{N_x}^{\rm peak}$ and $J_{N_x,N_y}^{\rm peak}$, and increase the residence time.

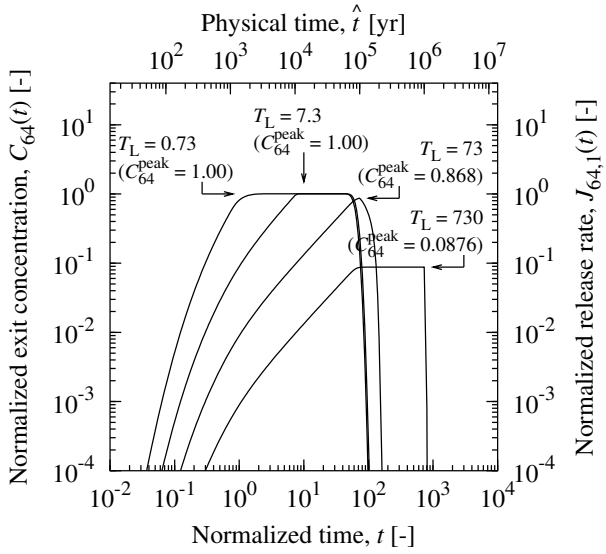

Figure 17 Normalized concentration $C_{64}(t)$ of cesium in the groundwater exiting the repository of configuration A and the corresponding normalized release rate $J_{64,1}(t)$ into the far field. Concentrations for leach time $T_{\rm L} = 0.73$, 7.3, 73, and 730 are plotted in solid lines.

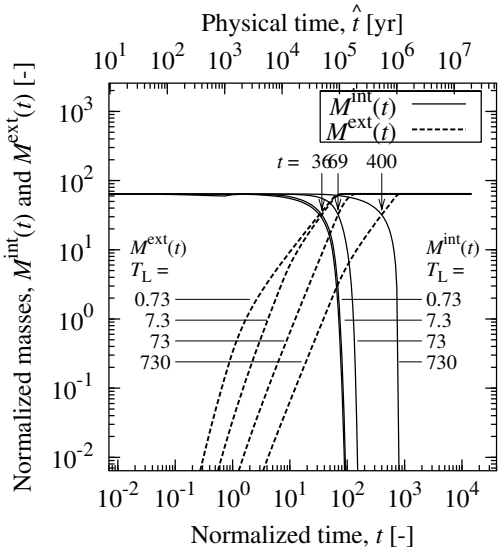

Figure 18 Normalized masses of cesium, $M^{\rm int}(t)$ in the repository and $M^{\rm ext}(t)$ in the far field for configuration A. Mass $M^{\rm int}(t)$ for leach time $T_{\rm L} = 0.73$, 7.3, 73, and 730 is plotted in solid lines. Mass $M^{\rm ext}(t)$ in the far field is plotted in dashed lines.

3.6 Capacity Extension of the Repository

In this section, we will observe effects of increased mass loading in the repository on $C^{\text{peak}}_{N_x}$, $J^{\text{peak}}_{N_x,N_y}$, and the representative residence time in the repository. The initial mass loading in the entire repository can be increased (a) by increasing the number of waste canisters, and (b) by increasing the mass loading in each canister.

3.6.1 Repository-Footprint Extension

We consider increasing the total number of waste canisters in the repository by changing values of N_x and N_y. Figures 19 and 20 show (N_x, N_y)-dependence of $C^{\text{peak}}_{N_x}$ and $J^{\text{peak}}_{N_x,N_y}$, respectively, for $T_{\text{L}} = 7.3$. The figure shows contour plots of $C^{\text{peak}}_{N_x}$ and $J^{\text{peak}}_{N_x,N_y}$ as functions of N_x and N_y based on formulae (29), (35), and (36).

The peak exit concentration $C^{\text{peak}}_{N_x}$ does not depend on N_y, and hence its value is determined only by N_x. The peak exit concentration $C^{\text{peak}}_{N_x}$ increases proportionally with N_x for $N_x < T_{\text{L}}$, and is constant at the upperbound value for $N_x > T_{\text{L}}$ as observed in Figure 9. Note that $C^{\text{peak}}_{N_x}$ is not affected either by N_x or by N_y if N_x is greater than T_{L}. It follows that, if N_x is greater than T_{L}, the change of the canister-array configuration does not affect $C^{\text{peak}}_{N_x}$, and that the number of canisters in the repository can be increased in both N_x and N_y directions without increasing $C^{\text{peak}}_{N_x}$.

The peak release rate $J^{\text{peak}}_{N_x,N_y}$, in contrast, increases proportionally with N_y. Increase in the number of canisters in any direction therefore leads to the increase in $J^{\text{peak}}_{N_x,N_y}$ for $N_x < T_{\text{L}}$. For $N_x > T_{\text{L}}$, repository can be extended in the x direction without increasing $J^{\text{peak}}_{N_x,N_y}$.

3.6.2 Increasing the Mass Loading in Each Canister

The dimensionless system given by Eqs. (5′) through (20′) is not involved with the initial mass loading per canister, $\hat{M}^{\circ}$. The effect of change in the initial mass loading by a factor of a appears in Eqs. (3′) and (4′); the right sides in Eqs. (3′) and (4′) are multiplied by the factor a.

The effect of increase in the initial mass loading on the exit concentration $C_{N_x}(t)$ is shown in Figures 21 and 22 for configurations A and C, respectively. Exit concentration $C_{N_x}(t)$ for the increased initial mass $10\hat{M}^{\circ}$ is shown

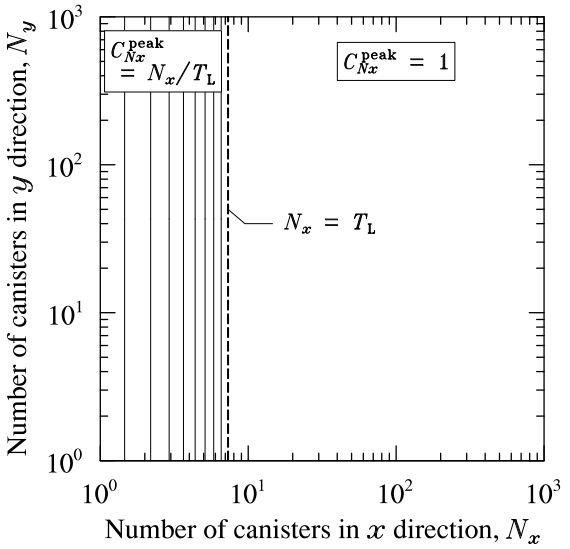

Figure 19 Dependence of the peak exit concentration $C^{\text{peak}}_{N_x}$ on the canister-array configuration (N_x, N_y) for $T_{\text{L}} = 7.3$. The contour levels are plotted in logarithmic scale.

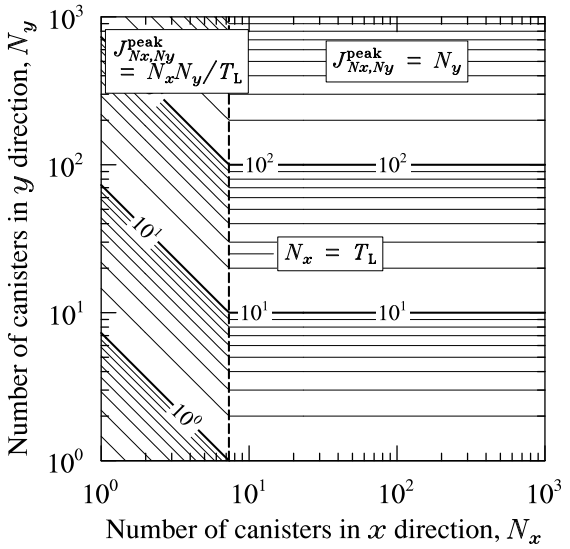

Figure 20 Dependence of the peak release rate $J^{\text{peak}}_{N_x,N_y}$ on the canister-array configuration (N_x, N_y) for $T_{\text{L}} = 7.3$. The contour levels are plotted in logarithmic scale.

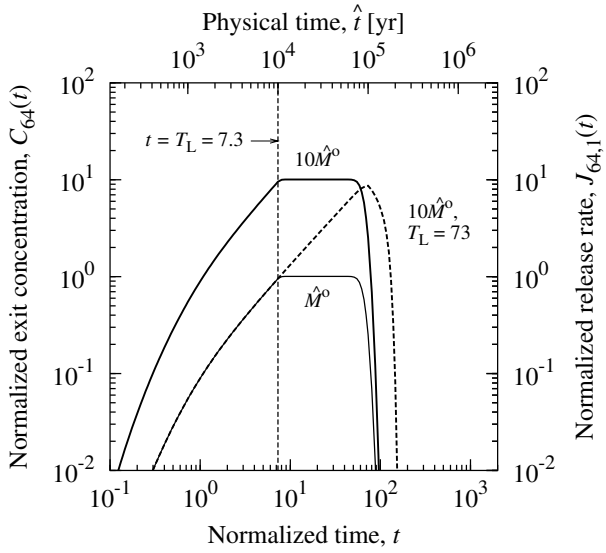

Figure 21 Effect of increase in the initial mass loading on the release from the repository of configuration A. The normalized exit concentration $C_{64}(t)$ and the normalized release rate $J_{64,1}(t)$ are shown for initial mass $\hat{M}^\circ$ and leach time $T_L = 7.3$ (thin solid line), initial mass $10\hat{M}^\circ$ and leach time $T_L = 7.3$ (thick solid line), and for initial mass $10\hat{M}^\circ$ and leach time $T_L = 73$ (dashed line).

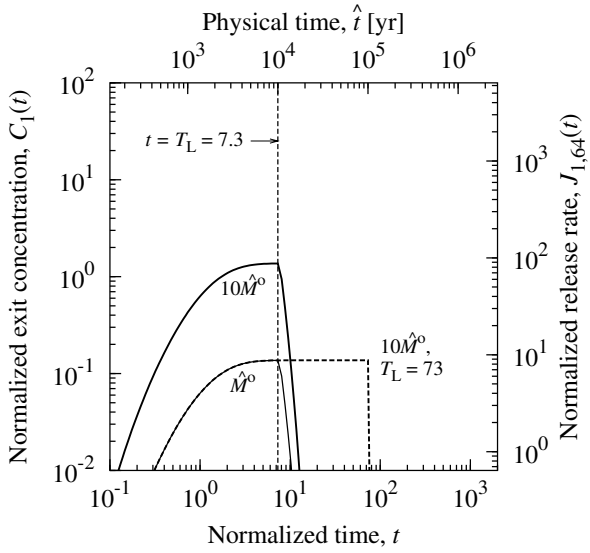

Figure 22 Effect of increase in the initial mass loading on the release from the repository of configuration C. The normalized exit concentration $C_1(t)$ and the normalized release rate $J_{1,64}(t)$ are shown for initial mass $\hat{M}^\circ$ and leach time $T_L = 7.3$ (thin solid line), initial mass $10\hat{M}^\circ$ and leach time $T_L = 7.3$ (thick solid line), and for initial mass $10\hat{M}^\circ$ and leach time $T_L = 73$ (dashed line).

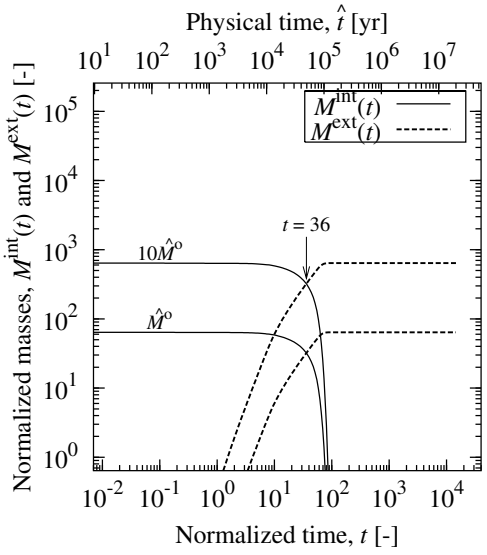

Figure 23 Effect of increase in the initial inventory per canister on the mass distribution for configuration A. The normalized mass $M^{int}(t)$ in the repository and $M^{ext}(t)$ in the far field are shown for initial mass $\hat{M}^\circ$ and $10\hat{M}^\circ$. The matrix leach-time is set to $T_L = 7.3$ for both cases.

in the figures together with that for the initial mass $\hat{M}^\circ$. It is observed that, in both configurations, the profile of $C_{N_x}(t)$ for $10\hat{M}^\circ$ is the same as that for $\hat{M}^\circ$ except that its magnitude is 10 times greater than the other. The peak exit concentration $C_{N_x}^{\text{peak}}$ and the peak release rate $J_{N_x,N_y}^{\text{peak}}$ are therefore increased by the factor of 10 as well regardless of the configuration.

The masses $M^{\text{int}}(t)$ and $M^{\text{ext}}(t)$ for configuration A are shown in Figure 23 with initial mass $\hat{M}^\circ$ and $10\hat{M}^\circ$. As observed in $C_{N_x}(t)$, the masses also increase by the factor of 10 when the initial mass is increased by the factor of 10. Thus, $C_{N_x}(t)$, $J_{N_x,N_y}(t)$, $M^{\text{int}}(t)$, and $M^{\text{ext}}(t)$ increase proportionally with the initial mass loading per canister. It is observed, however, that the residence time in the repository ($t = 36$ in Figure 23) is not affected by the initial-mass increase.

It has been observed in the previous sections that the elongation of the matrix leach time T_{L} reduces the peak exit concentration $C_{N_x}^{\text{peak}}$ if $T_{\text{L}} > N_x$. The leach-time elongation due to waste-form improvement may be an option for extending the repository capacity without increasing the environmental impact. The exit concentration $C_{N_x}(t)$ for the increased mass loading $10\hat{M}^\circ$ and leach time $T_{\text{L}} = 73$ is also shown in Figures 21 and 22. For both configurations A and C, the concentration $C_{N_x}(t)$ for increased mass and elongated leach time overlaps with that for the original mass $\hat{M}^\circ$ and leach time $T_{\text{L}} = 7.3$ at early times ($t < T_{\text{L}}$). For configuration C (Figure 22), the peak exit concentration $C_{N_x}^{\text{peak}}$ is observed to remain the same value after increasing the initial mass with leach-time elongation. We have observed in the previous sections that $C_{N_x}^{\text{peak}}$ is not reduced by leach-time elongation for configurations with $N_x > T_{\text{L}}$. For configuration A (Figure 21), the peak exit concentration $C_{N_x}^{\text{peak}}$ is not maintained at the same level after increasing the initial mass with leach-time elongation.

3.7 Effect of Radioactive Decay

The dimensionless system given by Eqs. (3′) through (20′) does not contain the information about radioactive decay of the radionuclide. In order to observe the effect of radioactive decay, the exit concentration $\hat{C}_{64}(\hat{t})$ for ^{135}Cs with its half-life 2.3×10^6 yr is depicted in Figure 24 together with that for the stable isotope ^{133}Cs and for

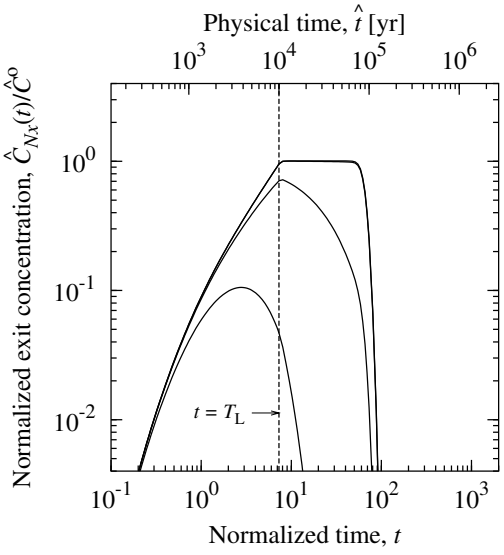

Figure 24 Effect of radioactive decay on the exit concentration. The normalized exit concentration $\hat{C}_{N_x}(t)/\hat{C}^\circ$ in configuration A is plotted for the stable isotope (^{133}Cs), isotope with half-life of 2.3×10^6 yr (^{135}Cs), isotope with the hypothetical half-life 2.3×10^4 yr and 2.3×10^3 yr. Matrix leach-time $T_{\text{L}} = 7.3$ is used.

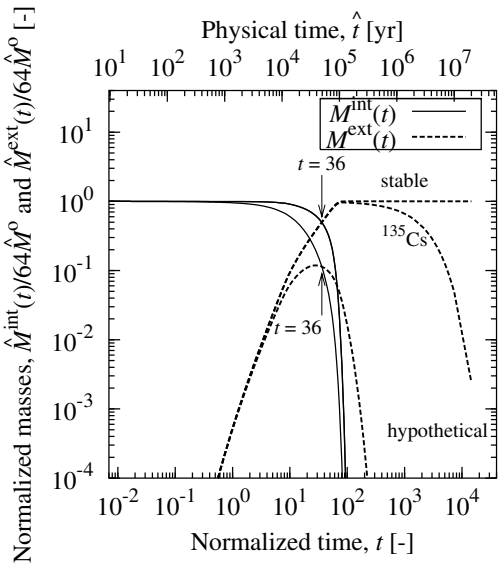

Figure 25 Effect of radioactive decay on the mass distribution. The normalized masses $\hat{M}^{\text{int}}(t)/64\hat{M}^\circ$ and $\hat{M}^{\text{ext}}(t)/64\hat{M}^\circ$ in configuration A is plotted for the stable isotope (^{133}Cs), isotope with half-life of 2.3×10^6 yr (^{135}Cs), and isotope with the hypothetical half-life 2.3×10^4 yr. Matrix leach-time $T_{\text{L}} = 7.3$ is used.

hypothetical isotopes with half-life 2.3×10^4 yr and 2.3×10^3 yr. Note that $\hat{C}_{N_x}(\hat{t})/\hat{C}^\circ$ for the stable isotope ($\hat{\lambda} = 0$) is identical to $C_{N_x}(t)$ in the dimensionless system [see Eq. (23g)]. Thus, the curve $\hat{C}_{64}(\hat{t})/\hat{C}^\circ$ for ^{133}Cs in Figure 24 is identical to $C_{64}(t)$ in Figure 6. Since the half-life of ^{135}Cs (2.3×10^6 yr) is far greater than the time domain of the radionuclide release, the effect of radioactive decay is hardly observed in $\hat{C}_{64}(\hat{t})$ for ^{135}Cs, and the curve $\hat{C}_{64}(\hat{t})$ for ^{135}Cs overlaps with that for ^{133}Cs. It follows that the discussions on $C_{N_x}(t)$ and $J_{N_x,N_y}(t)$ in the dimensionless system can be directly applied to the real quantities $\hat{C}_{N_x}(\hat{t})$ and $J_{N_x,N_y}(\hat{t})$ for a long-lived radionuclide if the decay effect is negligible during the time domain of release.

It is observed that the concentration profile deviates from that for the stable isotope ^{133}Cs as the half-life becomes shorter. The plateau is not observed for half-lives 2.3×10^4 yr and 2.3×10^3 yr because of the dominant effect of radioactive decay. For half-life 2.3×10^3 yr, the real peak of the exit concentration is observed before the plateau for ^{133}Cs begins. Thus, the discussions on the peak exit concentration in the dimensionless system may not directly correspond to the real peak concentration. However, the peak exit concentration given in Eq. (35), which corresponds to $\hat{C}^\circ$ [mol/m^3], still gives the conservative, upperbound value regardless of the half-life. The upperbound value $\hat{C}^\circ$ is realistic for long-lived radionuclides, and is more conservative for short-lived radionuclides.

Masses $\hat{M}^{\text{int}}(\hat{t})$ and $\hat{M}^{\text{ext}}(\hat{t})$ for configuration A are depicted in Figure 25 for the various half-lives. Mass profiles $\hat{M}^{\text{int}}(\hat{t})/64\hat{M}^\circ$ and $\hat{M}^{\text{ext}}(\hat{t})/64\hat{M}^\circ$ for ^{135}Cs overlap with those for the stable isotope ^{133}Cs until radionuclide release ceases at around 10^5 yr. The mass $\hat{M}^{\text{ext}}(\hat{t})/64\hat{M}^\circ$ of ^{135}Cs decreases thereafter by radioactive decay. For hypothetical half-life 2.3×10^4 yr, it is observed that a large portion of radionuclide decays within the repository, and the mass $\hat{M}^{\text{ext}}(\hat{t})/64\hat{M}^\circ$ does not reach unity. Note that the representative residence time is observed identical for all isotopes regardless of the half-life.

4 DISCUSSION

In the environmental impact assessment of geologic disposal of radioactive waste, analysis on radionuclide transport in the near field is important for the determination of the radionuclide concentration as the inlet boundary condition for the transport analysis in the far field. As observed in Figures 12 and 13, both the exit concentration $C_{N_x}(t)$ and the release rate $J_{N_x,N_y}(t)$ are not only affected by the total mass loading in the repository but also by the canister-array configuration (N_x and N_y). If $C_{N_x}(t)$ is used as the inlet boundary condition for the far-field analysis, the results of the far-field analysis also reflect the effect of canister-array configuration introduced by $C_{N_x}(t)$. The previous performance assessment,[3] that took into account radionuclide release only from a single waste canister, showed the difference originating in the total mass loading, but not that originating in the canister-array configuration.

Despite the fact that the exit concentration $C_{N_x}(t)$ is affected by the canister-array configuration, it has also been observed that $C_{N_x}(t)$ has a fixed upper bound which it never exceeds regardless of the number of canisters or of their configuration. If this upperbound concentration given by Eq. (35) is used as the input boundary condition for a transport analysis in the far field, the concentration in the far field can be conservatively overestimated. Since the upper bound is for all canister-array configurations, this conservative concentration in the far field can be estimated without specifying the configuration or the number of canisters in the repository. The upperbound concentration is determined by the initial mass loading of the radionuclide in a single canister, the volumes of the pore water in the buffer region and the NFR region of a compartment, and the sorption properties of the radionuclide in the media. Since it does not depend on the leach time T_{L} or on the groundwater-flow rate $\hat{F}$, it is free from the uncertainties originating in these parameter values.

4.1 Capacity Expansion

We have observed in Section 3.6 how the increased mass loading in the repository affects the exit concentration, the release rate, and the mass distributions. If the impact of the radionuclide release from the repository on the environment is measured on the basis of radionuclide mass such as M^{ext}, change in the impact can be crudely described by the change in the peak release rate $J^{\text{peak}}_{N_x,N_y}$ from the repository. We discuss on the ways to increase the total mass loading in the existing design of repository without increasing the peak release rate $J^{\text{peak}}_{N_x,N_y}$.

We assume that the repository site is fixed and that the geometry in a compartment remains the same as the original design of the repository. Therefore, the properties in the buffer region and the NFR region are the same as those in the original design.

If the number N_x of canisters in the flow direction is greater than the normalized leach time T_{L} in the original design, the peak release rate $J^{\mathrm{peak}}_{N_x,N_y}$ is insensitive to changes in N_x and T_{L}. Elongation of the leach time T_{L} due to waste-form improvement does not affect the peak release rate $J^{\mathrm{peak}}_{N_x,N_y}$ unless T_{L} becomes less than N_x. In such a case, the mass loading in the repository can be increased by increasing the number N_x of canisters in the groundwater-flow direction, without increasing $J^{\mathrm{peak}}_{N_x,N_y}$.

If N_x is less than T_{L} in the original design, $J^{\mathrm{peak}}_{N_x,N_y}$ is proportional to the total number of canisters in the repository, N_xN_y, and is inverse-proportional to the leach time T_{L}. Extension of the repository footprint (i.e., increase in the number of canisters) would lead to the increase in $J^{\mathrm{peak}}_{N_x,N_y}$ (regardless of whether to increase N_x or N_y) unless it is accompanied by the leach-time elongation. In order to keep $J^{\mathrm{peak}}_{N_x,N_y}$ from increasing, T_{L} must be made greater by the same factor as the increase in N_x. The total mass loading in the repository can be increased also by increasing the mass loading in each canister. Since the peak release rate increases proportionally to the mass increase, T_{L} must be made greater by the same factor or more in order to keep $J^{\mathrm{peak}}_{N_x,N_y}$ from increasing.

5 CONCLUSION

Radionuclide transport in a water-saturated repository has been investigated for a radionuclide congruently released from waste forms, with a model which takes into account spatial array configurations of multiple waste canisters. By numerical and analytical calculations, the concentration of a congruently released radionuclide at the repository exit is observed for various canister-array configurations. The peak concentration and the peak release rate at the repository exit have been analytically formulated.

It has been found that, if the repository length (i.e., the number of compartments) in the groundwater-flow direction is greater than a threshold value, the peak concentration of the radionuclide at the repository exit is equal to a theoretical upper-bound level. In such cases, the footprint of the repository can be extended without increasing the peak concentration at the repository exit, regardless of the number of canisters in the repository or the canister-array configuration. The upperbound concentration given by Eq. (35) is determined by the initial inventory of the radionuclide in a canister, sorption properties of the radionuclide, and the volumes of the NFR and buffer region of a compartment. This upperbound concentration can be used as the input boundary condition for far-field transport analyses of a congruently released radionuclide, which gives conservatively overestimated results for the concentration in the far field.

If the repository is not long enough to have the constant upperbound concentration, it is observed that the exit concentration and the release rate directly depend on the canister-array configuration and the matrix leach-time. In the comparison among different canister-array configurations, it is observed that the peak exit concentration is minimized by arranging canisters in a line perpendicular to the groundwater-flow direction. However, the peak release rate from the entire repository is minimized by arranging canisters in a line parallel to the flow direction. The perfomance evaluation of repository designs may thus vary depending on whether it is based on concentration or the release rate from the repository.

If the number of canisters connected in the flow direction increases, the effect of improving the waste matrix by increasing the leach time would be less effective in decreasing the peak exit concentration because the peak concentration is maintained at the upper-bound value. Because of the upperbound exit concentration, effects of the performance improvement of the waste-matrix as a barrier is not observed in the peak exit concentration, or in the peak release rate from the repository, unless the matrix leach-time becomes greater than a threshold value.

Magnitude of the peak exit concentration and the peak release rate increases proportionally with the initial mass loading per canister. The residence time of the nuclide in the repository is not affected by the initial inventory.

Thus, the present study shows that the peak exit concentration of a congruently released radionuclide will not always be proportional to the number of canisters, but is affected by the canister-array configuration and the leach time. If the radionuclide transport time in the repository is longer than the leach time, the peak exit concentration

becomes insensitive to the canister-array configuration and the leach time.

The present model is suitable in assisting in the design of a repository since the effects of the canister-array configuration is reflected by the peak exit concentration and the peak release rate.

A Details of Waste-Matrix Region

The initial mass $\hat{M}^{\circ}$ of the radionuclide in a single waste matrix is uniformly distributed over the volume $\hat{V}^{\circ}$ [m^3] of the waste matrix. It is assumed that dissolution of the waste matrices in all the compartments begins at time $\hat{t} = 0$ [yr]. Each waste matrix degrades at a constant volumetric rate until it completely dissolves in the groundwater at time $\hat{t} = \hat{T}_{\mathrm{L}}$. The volume $\hat{V}^{\mathrm{W}}(\hat{t})$ [m^3] of the matrix which remains intact at time $\hat{t}$ is given as

$$\hat{V}^{\mathrm{W}}(\hat{t}) = \begin{cases} \hat{V}^{\circ}(1 - \hat{t}/\hat{T}_{\mathrm{L}}), & 0 \le \hat{t} < \hat{T}_{\mathrm{L}}, \\ 0, & \hat{t} \ge \hat{T}_{\mathrm{L}}. \end{cases} \tag{37}$$

The initial concentration of the radionuclide in the matrix is given as $\hat{M}^{\circ}/\hat{V}^{\circ}$. The concentration $\hat{C}^{\mathrm{W}}(\hat{t})$ [mol/m^3] of the radionuclide contained in the intact matrix decreases with time due to radioactive decay, and is given as

$$\hat{C}^{\mathrm{W}}(\hat{t}) = e^{-\hat{\lambda}\hat{t}}\hat{M}^{\circ}/\hat{V}^{\circ}, \quad 0 \le \hat{t} < \hat{T}_{\mathrm{L}}, \tag{38}$$

where $\hat{\lambda}$ [yr^{-1}] is the radioactive decay constant ofthe radionuclide.

As the waste matrix degrades, the radionuclide is released congruently from the matrix. The radionuclide released from the matrix is assumed to dissolve immediately in the water phase at waste-matrix/buffer interface. The congruent release rate $\hat{q}(\hat{t})$ [mol/yr] is written as

$$\hat{q}(\hat{t}) = -\frac{\mathrm{d}\hat{V}^{\mathrm{W}}}{\mathrm{d}\hat{t}}\hat{C}^{\mathrm{W}}(\hat{t}) = \begin{cases} \hat{M}^{\circ}e^{-\hat{\lambda}\hat{t}}/\hat{T}_{\mathrm{L}}, & 0 < \hat{t} < \hat{T}_{\mathrm{L}}, \\ 0, & \hat{t} \ge \hat{T}_{\mathrm{L}}. \end{cases} \tag{39}$$

The mass $\hat{M}^{\mathrm{W}}(\hat{t})$ [mol] of the radionuclide in the intact waste matrix at time $\hat{t}$ is calculated as a product of $\hat{V}^{\mathrm{W}}(\hat{t})$ and $\hat{C}^{\mathrm{W}}(\hat{t})$, and is obtained as

$$\hat{M}^{\mathrm{W}}(\hat{t}) = \begin{cases} \hat{M}^{\circ}\left(1 - \hat{t}/\hat{T}_{\mathrm{L}}\right)e^{-\hat{\lambda}\hat{t}}, & 0 \le \hat{t} < \hat{T}_{\mathrm{L}}, \\ 0, & \hat{t} \ge \hat{T}_{\mathrm{L}}. \end{cases} \tag{40}$$

References

[1] J. AHN, D. KAWASAKI, and P. L. CHAMBRÉ, "Relationship among Performance of Geologic Repositories, Canister-Array Configuration, and Radionuclide Mass in Waste," *Nucl. Technol.*, **140**, *1*, 94 (2002).

[2] D. KAWASAKI, J. AHN, and P. L. CHAMBRÉ, "Analysis on Radionuclide Transport in a Repository with Multiple Canisters," *Proc. 9th Int. High-Level Radioactive Waste Management Conf.*, American Nuclear Society, Las Vegas (2001).

[3] *Second Progress Report on Research and Development for the Geological Disposal of HLW in Japan, H12: Project to Establish the Scientific and Technical Basis for HLW Disposal in Japan*, **3**, V, Japan Nuclear Cycle Development Institute, Tokai-Mura (2000).

[4] K. TSUJIMOTO, D. KAWASAKI, J. AHN, and P. L. CHAMBRÉ, "Virtual Repository (VR) Version 1.0 Operation Manual," Department of Nuclear Engineering, University of California, Berkeley (2000).

[5] J. AHN, "Criticality Safety Assessment for a Conceptual High-Level-Waste Repository in Water-Saturated Geologic Media," *Nucl. Technol.*, **126**, 303 (1999).